Planetary and Space Science 57 (2009) 1807–1812

Contents lists available at ScienceDirect

Planetary and Space Science

journal homepage: www.elsevier.com/locate/pss

Characteristics of charged dust inferred from the Cassini RPWS measurements in the vicinity of Enceladus

V.V. Yaroshenko [a], S. Ratynskaia [b,*], J. Olson [b], N. Brenning [b], J.-E. Wahlund [c], M. Morooka [c], W.S. Kurth [d], D.A. Gurnett [d], G.E. Morfill [a]

[a] Max-Planck-Institut für extraterrestrische Physik, D-85741 Garching, Germany
[b] Space and Plasma Physics, Royal Institute of Technology (KTH), Teknikringen 31, SE-100 44 Stockholm, Sweden
[c] Swedish Institute of Space Physics, Uppsala, Sweden
[d] Department of Physics and Astronomy, University of Iowa, Iowa City, IA 522 42, USA

ARTICLE INFO

Article history:
Received 1 December 2008
Received in revised form
3 March 2009
Accepted 5 March 2009
Available online 13 March 2009

Keywords:
Saturn moons
E-ring
Cassini
Dust size distribution
Dusty plasma

ABSTRACT

The data obtained by the Cassini Radio and Plasma Wave Science (RPWS) instrument during the shallow (17.02.2005) and the steep (14.07.2005) crossings of the E-ring revealed a considerable electron depletion in proximity to Enceladus's orbit (the difference between the ion and electron densities can reach $\sim 70\,\mathrm{cm}^{-3}$). Assuming that this depletion is a signature of the presence of charged dust particles, the main characteristics of dust down to *submicron* sized particles are derived. The differential size distribution is found to be well described by a power law with an index $\mu \sim 5.5-6$ for the lower size limit $a_{\min} = 0.03\,\mu\mathrm{m}$ and $\mu \sim 7.3-8$ for $a_{\min} = 0.1\,\mu\mathrm{m}$. The calculated average integral dust number density is weakly affected by values of μ and $a_{\min}$. For $a \gtrsim 0.1\,\mu\mathrm{m}$, both flybys gave the maximum dust density about $0.1-0.3\,\mathrm{cm}^{-3}$ in the vicinity of Enceladus. Our results imply that the dust structure near Enceladus is characterized by approximately the same vertical length scale of 8000 km and reaches a maximum at the same radial distance (displaced outward of the orbit of Enceladus) as found by Kempf et al. [2008. The E-ring in the vicinity of Enceladus. Spatial distribution and properties of the ring particles. Icarus 193, 420–437], from the dust impact data.

1. Introduction

Saturn's faint E-ring is the largest ring of the Solar System and extends from about $3R_S$ to at least $8R_S$, where $R_S = 60\,330$ km is the radius of Saturn. It mainly consists of submicron to micron sized icy grains (e.g. according to Nicholson et al., 1996, the size spectrum ranges mainly between 0.3 and 3 μm). There are at least four icy moons embedded in this ring: Mimas ($r_M = 3.07R_S$), Enceladus ($r_E = 3.95R_S$), Tethys ($r_T = 4.88R_S$), and Dione ($r_D = 6.25R_S$). Though all of them can serve as sources of dust, due to impactor-ejecta processes, the moon Enceladus has long been considered to be a main dust source in Saturn's E-ring. This was supported by the observations that the ring's optical depth peaks close to the orbit of this moon. The Enceladus flybys of the Cassini spacecraft provide a new insight into the origin and sustainment of Saturn's E-ring. Beyond the widely accepted dust production caused by micrometeoroid impacts on the atmosphereless satellites (the impactor-ejecta process), "geophysical" activities have been detected at the south pole of Enceladus, providing an additional, efficient dust source (Spahn et al., 2006a, Schmidt et al., 2008, Nature). Furthermore, Cassini's dust detector (CDA) and the radio and plasma wave science (RPWS) instrument, both have registered peaks of micron sized particles in proximity to Enceladus during the close flybys at this moon (Kurth et al., 2006; Kempf et al., 2008), thus supporting the idea of the exceptional role of this icy moon in dust production.

Most experiments to measure dust impacts on space missions have a cutoff for small particles sizes which cannot be reliably detected. The high rate detector of Cassini's CDA instrument registers particles of radii $a \gtrsim 1\,\mu\mathrm{m}$, while the main detector DA (dust analyzer) is capable to detect smaller grains. However, due to the instrument dead time of 1 s the DA cannot determine the dust number density within the dense E-ring (Srama et al., 2004; Kempf et al., 2008). The RPWS instrument is also sensitive only to the grains larger than a few microns (Gurnett et al., 2004; Kurth et al., 2006). Therefore, neither the CDA nor the RPWS dust measurements can be used directly to reconstruct the size distribution of submicron grains, which are mainly responsible for the ring's brightness (Kempf et al., 2008). For "larger", micron particles, the differential size distributions inferred from the dust detector and RPWS data are well described by a power law $dn_d \sim a^{-\mu}\,da$. During most of the crossings in the vicinity of

* Corresponding author.
E-mail address: srat@kth.se (S. Ratynskaia).

0032-0633/$ - see front matter © 2008 Elsevier Ltd. All rights reserved.
doi:10.1016/j.pss.2009.03.002

Enceladus, the power law index μ inferred from CDA measurements was found to be $4.8<\mu<5.4$ (Kempf et al., 2008) and the first RPWS dust impact data yielded $\mu \simeq 6.4 \pm 1.0$ (Kurth et al., 2006).

The Cassini RPWS instrument also provides measurements of basic parameters of the magnetospheric plasma. Knowledge of the ambient plasma is essential for modeling the grain charging (see Horányi, 1996). So far all theoretical studies of the E-ring dynamics were based on the plasma model derived by Richardson (1995) from the Voyager data. Early measurements by the Cassini plasma instruments (Sittler et al., 2005) in some places deviated significantly from the predictions of the Richardson model. Rather high negative dust equilibrium potential inferred from the dust charge measurements by CDA (at least for distances $r<5R_S$, see Kempf et al., 2006) as well as from measurements of the spacecraft potential by the RPWS Langmuir probe (LP) (Wahlund et al., 2005, 2009) were also not consistent with the Richardson model.

In this paper, we assume that the measured profiles of the plasma parameters near to the moon Enceladus bear imprint of the dust distribution around its source, where the dust number density is expected to be significantly higher than that within the main part of the E-ring. We use the data obtained during one shallow (17.02.2005) and one steep (14.07.2005) flyby. For both Cassini passages, the LP measurements reveal considerable electron depletion, while simultaneous measurements of the CDA gave the peak number density of dust particles near the moon. Note that the electron depletion has been also reported by Farrell et al. (2009), based on plasma wave measurements. Following analogy with usual complex plasmas, where the negatively charged dust can lead to significant electron depletion (Fortov et al., 2005), we associate the observed effect with an increase in charged dust density. The link between the two independent RPWS and CDA data allows us to reconstruct the size distribution down to submicron range, i.e. outside the cutoff for dust impact sensors. We also estimate the integral dust number density, n_d, and specify the characteristic length scales of the dust structure formed around the orbit of Enceladus.

2. Observations

After the Cassini orbit insertion in July 2004, the spacecraft performed a number of equatorial as well as steep traversals through the E-ring inside the orbit of the icy moon Dione. For a summary of crossing parameters and for geometry of passages we refer to Table 2 and Fig. 1 in Kempf et al. (2008), respectively. Here we focus on the measurements obtained during two E-ring passages where simultaneous reliable dust detector (Kempf et al., 2008) and plasma RPWS (Wahlund et al., 2009) measurements are available.

On February 17, 2005, Cassini passed the ring plane close to the orbit of Mimas at $\sim 3.5R_S$ and performed a close flyby of Enceladus during the outbound leg of her orbit, moving then with a small inclination along the ring plane (orbit 3). The elevation over the equatorial plane was around $0.02R_S$ in proximity to Enceladus's orbit. The closest approach to the moon surface was 1264 km, which is outside Enceladus's sphere of gravitational influence (the latter is characterized by a so called Hill radius, ~950 km, Spahn et al., 2006a). One can therefore expect that such shallow traversal as the flyby in orbit 3, can give an insight into the radial distribution of the dust within the E-ring, and in particular in proximity to Enceladus's orbit.

During the encounter on July 14, 2005 (orbit 11), Cassini passed the ring plane very steep (the piercing angle $\sim 53^\circ$) at $\sim 3.95R_S$, in the direct vicinity of the orbit of Enceladus (closest approach to the moon was 168 km above its surface). This steep passage through the ring plane is particularly useful for the understanding of vertical scales of the dust distribution formed around the orbit of the moon.

We now briefly review the principal features of RMSR and CDA data relevant for this paper.

2.1. RPWS plasma observations

Here we use the LP data from RPWS instrument. The plasma parameters are inferred from the LP current–voltage characteristics as described by Wahlund et al. (2005, 2009).

The electron n_e and ion n_i number densities and the probe floating potential U_{fl} for both of Cassini's flybys are shown in Figs. 1(a, b) and 2(a, b). Note that our data for the shallow passage relate to the outbound leg of the spacecraft trajectory, when Cassini performed a close flyby at Enceladus (during the inbound leg no significant electron depletion was registered). The ion densities are derived for average ion mass of 18 amu (Wahlund et al., 2009).

As seen from the figures, the data acquired during the two different geometries of the ring plane crossing are consistent with respect to the significant electron depletion near to the orbit of the

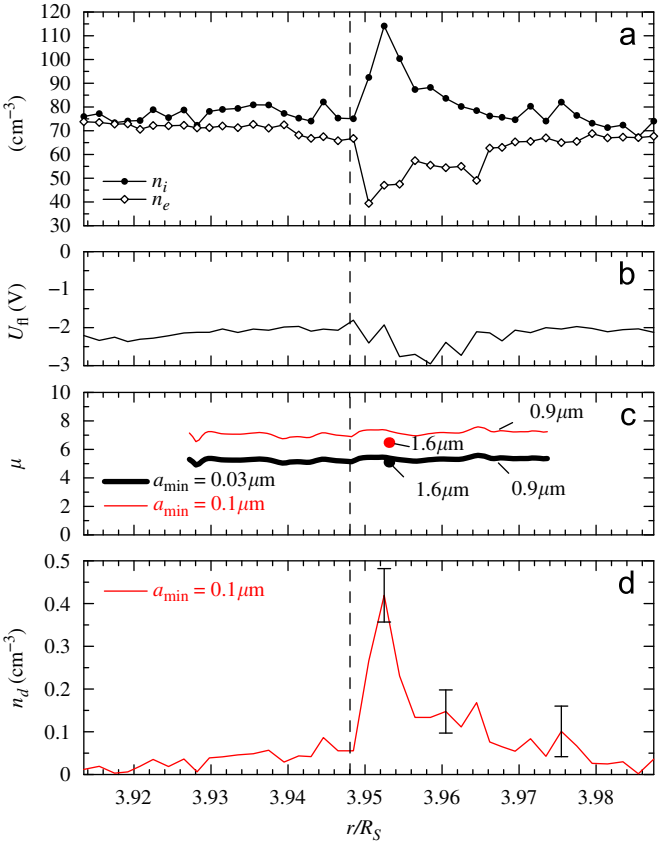

Fig. 1. RPWS measurements and dust characteristics during the close flyby at the orbit of Enceladus on July 14, 2005 (a vertical dashed line indicates the position of the closest approach to Enceladus). (a) The electron, n_e, and ion, n_i, number densities versus the distance to Saturn's rotation axis. (b) The probe floating potential, U_{fl} versus the radial distance. (c) The index of the differential size distribution, $\mu(r/R_S)$ obtained at $a_{thresh} = 0.9\,\mu m$ versus the distance to Saturn's rotation axis. Estimates for $a_{min} = 0.1\,\mu m$ are shown in red (gray) and for $a_{min} = 0.03\,\mu m$ in black. The points indicate sensitivity of μ to larger value of $a_{thresh} = 1.6\,\mu m$. (d) The integral dust number density profile, $n_d(r/R_S)$, calculated from Eq. (6) for the lower size limit $a_{min} = 0.1\,\mu m$. An error bar in the dust density due to uncertainties in measurements of $(n_i - n_e)$ is indicated. (For interpretation of the references to color in this figure legend, the reader is referred to the web version of this article.)

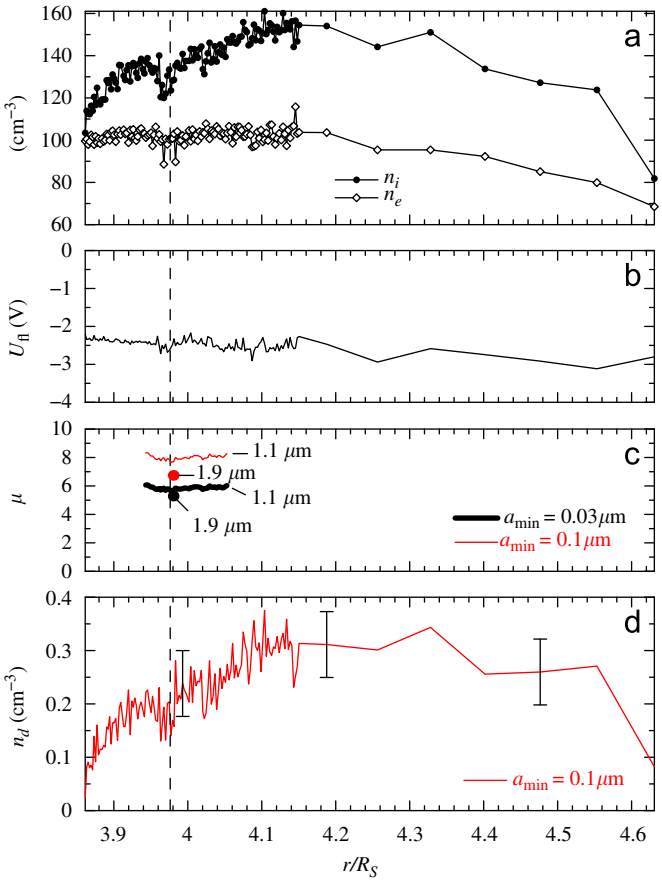

Fig. 2. RPWS measurements and dust characteristics during the close flyby at the orbit of Enceladus on February 17, 2005 (a vertical dashed line indicates the position of the closest approach to Enceladus). (a) The electron, n_e, and ion, n_i, number densities versus the distance to Saturn's rotation axis. (b) The probe floating potential, U_{fl} versus the radial distance. (c) The index of the differential size distribution, $\mu(r/R_S)$ obtained at $a_{thresh} = 1.1\,\mu$m versus the distance to Saturn's rotation axis. Estimates for $a_{min} = 0.1\,\mu$m are shown in red (gray) and for $a_{min} = 0.03\,\mu$m in black. The points indicate sensitivity of μ to larger value of $a_{thresh} = 1.9\,\mu$m. (d) The integral dust number density profile, $n_d(r/R_S)$, calculated from Eq. (6) for the lower size limit $a_{min} = 0.1\,\mu$m. An error bar in the dust density due to uncertainties in measurements of $(n_i - n_e)$ is indicated. (For interpretation of the references to color in this figure legend, the reader is referred to the web version of this article.)

moon Enceladus. On the other hand, these plasma variations develop on quite different characteristic length scales. The steep crossing, Fig. 1, reveals: (i) the large scale length of the electron depletion of about 5000−6000 km (a corresponding vertical scale is up to $\Delta z \simeq 8000$ km), (ii) a sharp local increase of the electron depletion, up to $n_i - n_e \simeq 70\,\mathrm{cm}^{-3}$, in the direct vicinity of the moon within the radial scale of 600 km (the vertical thickness about 800 km). Contrary to the steep crossing, the shallow passage (Fig. 2) reveals a more extensive range of electron depletion: it appears at $r \simeq 3.9R_S$, exhibits a not pronounced maximum within $r \simeq 4.1 - 4.3R_S$ and extents up to $r \simeq 4.6R_S$.

2.2. CDA data

For both the shallow and the steep flybys the dust impact data are available within the range of $3.92 < r/R_S < 4.05$ (Kempf et al., 2008). By means of plausible assumptions about the particle size distribution it became possible to transform the measured impact rates into number densities of grains larger than a given size. The results are presented in Fig. 10 for the orbit 11 and Figs. 9 and 11 for the orbit 3 in Kempf et al. (2008).

For grains exceeding 0.9 and 1.6 μm, Kempf et al. (2008) derived a power low differential size distribution with slope indices in a range of $4.8 \lesssim \mu \lesssim 5.4$. These values imply that the main contribution to the mass as well as the geometric cross section of the ring is due to smaller dust grains. The model predicted the maximum number density in the vicinity of Enceladus to be in the range of $(1.6-2.1)\times 10^{-7}\,\mathrm{cm}^{-3}$ for grains larger than 0.9 μm, and of $(2.1-7.6)\times 10^{-8}\,\mathrm{cm}^{-3}$ for grains larger than 1.6 μm. Kempf et al. (2008) concluded that Enceladus feeds a torus populated by micron sized grains along its orbit. The CDA measurements have also been used for the determination of the ring structure near the orbit of Enceladus. Kempf et al. (2008) reported that the vertical ring structure fits well a Gaussian distribution with the full-width-half-maximum of ~4000 km, which is consistent with earlier estimates of Kurth et al. (2006). Such a characteristic thickness is in excellent agreement with the large scale vertical length of the electron depletion region inferred from the LP data during the flyby in orbit 11 ($\Delta z \simeq 8000$ km).

3. Equations of the problem and the effects of a dust size distribution

In this section we consider some important effects of the dust size distribution on the grain charging. Dust grains in space come in all sizes and can be described by a continuous spectrum in a certain size range. Both RPWS and CDA measurements based on the impact data within the E-ring showed that the differential dust spectrum is described best by a power law size distribution. We also accept this general form

$$dn_d = W(a)\,da = Ka^{-\mu}\,da, \quad a_{min} \leqslant a \leqslant a_{max}, \tag{1}$$

but keep the index μ as a free parameter. The total dust number density is given by

$$n_d = \int_{a_{min}}^{a_{max}} W(a)\,da = \frac{K}{1-\mu}(a_{max}^{1-\mu} - a_{min}^{1-\mu}). \tag{2}$$

For the studied conditions, the inequality $a \ll \lambda_D$, where λ_D is the Debye screening length, is fulfilled and thus the standard charging model (see, e.g. Fortov et al., 2005) can be used, leading to the particle charge $q(a) = 4\pi\varepsilon_0 Ua$. Here U is the electric surface potential, which is assumed to be independent of size (equal for all dust grains). The validity of this assumption has been recently demonstrated in the E-ring at least at distances of $r < 5R_S$, where the particle potential reasonably agrees with the spacecraft potential (Kempf et al., 2006). Moreover, the assumption on the size independent surface potential can be also supported by a fact that we deal with the cold ($T_e \sim$ a few eV) thermal plasma (Wahlund et al., 2009; Jacobsen et al., 2009) and, hence, the effect of secondary electron emission which could result in a dependence $U(a)$ is negligible (Chow et al., 1993). One can therefore define the total charge density carried by the dust grains as

$$\rho_d = 4\pi\varepsilon_0 U \int_{a_{min}}^{a_{max}} W(a)a\,da = \frac{4\pi\varepsilon_0 KU}{2-\mu}(a_{max}^{2-\mu} - a_{min}^{2-\mu}). \tag{3}$$

On the other hand, the charge balance requires

$$\rho_d = q_e(n_e - Z_i n_i) \tag{4}$$

thus leading to the relation between the total dust density, n_d and the electron depletion

$$4\pi\varepsilon_0 U \frac{1-\mu}{2-\mu}\frac{a_{max}^{2-\mu} - a_{min}^{2-\mu}}{a_{max}^{1-\mu} - a_{min}^{1-\mu}} n_d = q_e(n_e - Z_i n_i). \tag{5}$$

Here q_e is the elementary charge and Z_i an ion charge number. Since usually $a_{min} \ll a_{max}$, a further simplification for $\mu \gg 1$ then

gives the total dust density

$$n_d \simeq \frac{q_e(n_e - Z_i n_i)}{q_{min}} \frac{2-\mu}{1-\mu}, \quad (6)$$

where we introduce the charge carried by the smallest grains $q_{min} = 4\pi\varepsilon_0 U a_{min}$.

Expression (6) has a simple physical meaning: for any steep dust size distribution ($\mu \gg 1$), the results are heavily weighted towards the smaller sized grains, and mainly these particles provide the plasma quasineutrality.

Finally keeping the available RPWS and CDA dust impact measurements in mind (Kurth et al., 2006; Kempf et al., 2008) we introduce the partial dust density, corresponding to a certain threshold value, a_{thresh} (with $a_{max} > a_{thresh} > a_{min}$) as

$$n_{d,part} = \int_{a_{thresh}}^{a_{max}} W(a)\,da \quad (7)$$

or more explicitly for $Z_i = 1$

$$n_{d,part} = \frac{q_e(n_e - n_i)}{4\pi\varepsilon_0 U} \frac{2-\mu}{1-\mu} \frac{a_{max}^{1-\mu} - a_{thresh}^{1-\mu}}{a_{max}^{2-\mu} - a_{min}^{2-\mu}}. \quad (8)$$

Solving Eqs. (5) and (8) allows us to find the slope indices μ and the total dust density n_d as functions of radial distances from Saturn, r/R_S.

4. Results

The micron sized grains have the maximum dust density of $10^{-7}\,cm^{-3}$ (Kempf et al., 2008) and thus cannot alone cause the significant electron depletion (unless the particles carry unreasonably high charges). To explain the RPWS findings on divergent character of the electron and ion density profiles, we thus have to extend the dust size distribution down to submicron range.

With profiles of n_e and n_i (Figs. 1(a) and 2(a)) and CDA estimates of $n_{d,part}$, for several a_{thresh}, shown in Figs. 10(a) and 11(a) by Kempf et al. (2008), we solve Eq. (8) using $U \simeq U_{fl}$ (Figs. 1(b) and 2(b)). The calculated index profile $\mu(r/R_S)$ for the steep and shallow ring plane crossings are shown in Figs. 1(c) and 2(c), respectively. Note that the plots are given within the narrow range of the radial distances in the vicinity of the orbit of Enceladus. Such a restriction results from the availability of the dust impact data and corresponds to the radial distances presented in Figs. 10 and 11 of Kempf et al. (2008). To test a dependence of $\mu(r/R_S)$ on the low limit in the size spectrum, we consider two different a_{min}, taking a typical value $a_{min} = 0.1\,\mu m$ and a rather small one $a_{min} = 0.03\,\mu m$. Furthermore for the calculation of $\mu(r/R_S)$, we use $n_{d,part}$, corresponding to the most reliable CDA data, namely $a_{thresh} \simeq 1.1\,\mu m$ (flyby in orbit 3) and $a_{thresh} \simeq 0.9\,\mu m$ (flyby in orbit 11). The points introduced in the plots indicate sensitivity of $\mu(r/R_S)$ to other thresholds (taken from Kempf et al., 2008).

As seen from the figures, the estimates of the slope index for two different geometries of the crossings agree reasonably well at a given a_{min}: the average value corresponds to $\overline{\mu} \simeq 5.5$ (orbit 11) and $\overline{\mu} \simeq 6$ (orbit 3) for $a_{min} = 0.03\,\mu m$ and $\overline{\mu} \simeq 7.3$ (orbit 11) and $\overline{\mu} \simeq 8$ (orbit 3) for $a_{min} = 0.1\,\mu m$. The obtained size slope indices in general are slightly larger than $4.8 \lesssim \mu \lesssim 5.4$ derived from CDA data by Kempf et al. (2008), but reasonably match the estimates of $\mu \simeq 6.4 \pm 1.0$ inferred from RPWS dust impact measurements by Kurth et al. (2006).

For the calculated $\mu \sim 5.5-8$, the results for the total dust density are not sensitive to the upper limit in the particle spectrum (in the assumption that a_{max} exceeds a few microns), so n_d can be determined from the simple expression (6) with a high accuracy. Moreover, as seen from Eq. (6), the dust density is not very sensitive to μ either, and scales inversely with a_{min}.

Figs. 1(d) and 2(d) present the total number density profiles corresponding to the typical value of $a_{min} = 0.1\,\mu m$. To obtain n_d from Eq. (6), we used the above mentioned values of $\overline{\mu}$ within the same distance range as n_e and n_i profiles.

Our estimates inferred from the steep flyby in orbit 11, reveal a local increase of the dust density with $n_{d,max}/\overline{n}_d \simeq 5-8$ developing on a vertical length scale of order of 800 km (an equivalent radial length scale is of 500 km) near the orbit of Enceladus (Fig. 1(d)). Furthermore, our data indicate some vertical/radial asymmetry in the dust density distribution: the average values of n_d before and after the closest approach at Enceladus do not coincide (see Fig. 1(d)). The peak of the dust number density occurs about 45–50 s before the closest approach to the moon surface. The CDA measurements showed the peak impact rate of micron grains about 60 s before the closest approach to the moon surface, when Cassini just crossed the Hill sphere of Enceladus. Thus, the fact that n_d inferred from the two simultaneous, but physically independent measurements of the steep flyby, peaks approximately at the same radial distance displaced outward of the orbit of Enceladus by about $0.03-0.05R_S$ is noteworthy.

Earlier Spahn et al. (2006b) showed that a temporal offset of the peak impact rate with respect to the closest approach can be an indicator of a localized collimated dust source on the moon. The latter means that the distinct peak of the charged dust density before the closest approach to Enceladus in Fig. 1(d) might be an imprint of the moon's plumes emerging from the moon's south pole region. Furthermore the particles injected by the moon can have the largest initial vertical speeds within the inertial frame of the ring and thus have the large initial orbit inclinations. This might be a reason of the asymmetry in the dust density distribution observed during the steep flyby.

The particle number density derived from the flyby in shallow orbit 3 demonstrates a smeared profile of the dust population. It develops on the characteristic length scale about $0.7R_S \sim 4 \times 10^4$ km. Similar to CDA dust measurements during the shallow crossing, the densest region also falls outside of the orbit of Enceladus. Our results reveal an outward shift of the densest point, up to $(0.2-0.3)R_S$, with respect to the moon's orbit. The obtained shift is consistent with results of Kempf et al. (2008) and agrees well with position of the ring's peak brightness: de Pater et al. (2004) reported an outward shift of the peak brightness by about $0.25R_S$ with respect to the orbit of Enceladus. Note that this effect cannot be attributed to the particles' non-zero eccentricity but requires an outward transport of small dust grains injected by the moon (Juhász et al., 2007; Horányi et al., 2008).

The results for the integral dust density from the two flybys appear to be consistent if we compare the geometry of both Cassini trajectories and the position of Enceladus. During the steep crossing the spacecraft was near the moon slightly below the ring plane and elevation of the dust density up to its peak value $n_d \sim 0.3-0.4\,cm^{-3}$ occurs before encounter (to the right of dashed line in Fig. 1(d)). After the closest approach one finds much smaller dust density $n_d \lesssim 0.05\,cm^{-3}$, which could be associated with the background (equilibrium) dust. One can speculate that this, $n_d \lesssim 0.05\,cm^{-3}$, value is representative for the density in whole torus populated by dust fed by Enceladus along its orbit. During the shallow passage Cassini performed a close flyby at the moon during the outbound leg of the trajectory, and we find an average value of $n_d \sim 0.1-0.3\,cm^{-3}$ to the right of dashed line in Fig. 2(d), which agrees well with the values to the right of the peak in Fig. 1(d). Hence, one can conclude such enhanced dust densities observed during two independent flybys can be caused by the particles injected by Enceladus. We cannot directly compare the obtained values of the dust densities $n_d \sim 0.1-0.3\,cm^{-3}$ with CDA measurements since during all passages the smallest detectable by the CDA instrument particle size was 0.9 μm (Kempf et al.,

2008). The formal extension of the dust size distributions of Kempf et al. (2008) down to submicron grains ($a_{\min} = 0.1\,\mu$m) gives as a maximum $n_d \sim 0.015\,\mathrm{cm}^{-3}$, which is only one order of magnitude smaller than our predictions. On the other hand, a theoretical model for the formation of Enceladus's dust plume particles predicts a few orders of magnitude lower dust density for $a \gtrsim 0.1\,\mu$m (Schmidt et al., 2008, Nature, Fig. 3b). Such discrepanciescan be attributed to a fact that the model calculations were adjusted to the CDA measurements and took into account the ring background due to the grains $a \gtrsim 0.8\,\mu$m. The inclusion of the background due to smaller, submicron, grains could reconcile the discrepancies at least partially. In addition, note that although the model spectrum of Fig. 3b of Schmidt et al. (2008), gives much smaller numbers of the cumulative dust density it reproduces exactly the same slope $n_d \propto a_{\min}^{-1}$ within the range $0.1\,\mu\mathrm{m} \gtrsim a \gtrsim 1\,\mu$m as results from Eq. (6).

Although we have demonstrated that a simple model of charged dust matches well two independent series of the plasma data, we now discuss the physical restriction of the model. In general, the particle electric potential depends on the dust number density: its increase can lead to significant decrease in the absolute value of the electrostatic potential as compared to $|U|$ characteristic for an individual particle. For a dense dusty plasma, the influence of high n_d has been quantified by Goertz and Ip (1984). The results have been expressed as a function of the parameter $\chi = 4\pi n_d \lambda_D^2 a$. When $\chi \gg 1$, the surface potential decreases dramatically, while for small $\chi \ll 1$, the effect becomes negligible. Taking the typical value of the screening length in the E-ring $\lambda_D \simeq 1\,\mathrm{m}$ and $n_d \simeq 0.1\,\mathrm{cm}^{-3}$ yields $\chi \simeq 0.1$. One can conclude therefore that the surface potential under conditions studied is not significantly affected by high n_d.

5. Summary

In this paper, the plasma parameters obtained from the RPWS instrument, complemented by the dust impact (CDA) data for two Cassini's passages through the inner E-ring, both within proximity of the icy moon Enceladus, $3.9 < r/R_S < 4.6$, have been used. During both flybys, the RPWS measurements reveal considerable electron depletion up to $50-70\,\mathrm{cm}^{-3}$, while simultaneous CDA measurements gave the peak number density of dust particles near the moon. Following analogy with usual complex/dusty plasmas, where the negatively charged dust can lead to significant electron depletion, we associate the observed effect with an increase in charged dust density. To explain the RPWS data on divergent character of the electron and ion densities, we had extended the dust size distribution down to submicron range. It turned out that such grains carrying reasonable electron charges (up to a few tens—hundred electrons) able to provide the observed electron depletion.

Using the link between the two independent RPWS and CDA data, we have found quite high index of $\mu \sim 5.5-8$ which implies a very steep size distribution and provides predominance of small particles near the orbit of Enceladus. According to our results we can recognize a rather high background ring dust density, $n_d \lesssim 0.05\,\mathrm{cm}^{-3}$, and regions of the enhanced particle density, $n_d \sim 0.1-0.3\,\mathrm{cm}^{-3}$, in the direct vicinity of Enceladus, which can be associated with injected grains. The derived size distribution of the background E-ring particles seems to concur with the size distribution of the plume particles—we find similar value of μ in the regions with background as well as with elevated dust densities. It is noteworthy that the dust densities' estimations for both steep and shallow flybys give consistent results. Our results imply also that the dust structure near Enceladus is characterized by approximately the same vertical length scale of 8000 km and reaches a maximum at the same radial distance (displaced outward of the orbit of Enceladus) as follows from the dust impact data.

Although we have demonstrated that a simple model of charged dust works well at matching the RPWS plasma data of the two different Cassini flybys, our conclusions are based on limited observations. Other Cassini's trajectories should be analyzed to test our predictions of a rather higher density of submicron grains in the vicinity of Enceladus, to gain more statistics and to specify the spatial dust distribution in more detail. Among the questions that need to be addressed are also the main physical processes which determine the life cycle of the grains injected by Enceladus. To understand whether any processes favor submicron sized grains, one needs to involve the problems of gravitoelectrodynamics (Goertz, 1989; Bliokh et al., 1995; Horányi et al., 2008), when dynamics and spatial distribution of such small and highly charged particles are governed not only by gravitational but also electromagnetic, plasma drag forces, radiation pressure, etc.

Acknowledgments

The Swedish National Space Board (SNSB) supports the RPWS LP instrument onboard Cassini. V.V.Y. and S.R. acknowledge the support from The Royal Swedish Academy of Sciences.

References

Bliokh, P.V., Sinitsyn, V.G., Yaroshenko, V.V., 1995. Dusty and Self-Gravitational Plasmas in Space. Kluwer, Dordrecht.
Chow, V.W., Mendis, D.A., Rosenberg, M., 1993. Role of grain size and particle velocity distribution in secondary electron emission in space plasmas. J. Geophys. Res. 98, 19065–19076.
Farrell, W.M., Kurth, W.S., Gurnett, D.A., Johnson, R.E., Kaiser, M.L., Wahlund, J.-E., Waite, J.H., Jr., 2009. The electron density dropout near Enceladus in the context of water–vapor and water–ice. Geophys. Res. Lett., in press (2008GL037108R).
Fortov, V.E., Ivlev, A.V., Khrapak, S.A., Khrapak, A.A., Morfill, G.E., 2005. Complex (dusty) plasmas: current status, open issues, perspectives. Phys. Rep. 421 (1–2).
Goertz, C.K., 1989. Dusty plasmas in the Solar System. Rev. Geophys. 27, 271–292.
Goertz, C.K., Ip, W.H., 1984. Limitation of electrostatic charging of dust particles in a plasma. Geophys. Res. Lett. 11, 349–352.
Gurnett, D.A., Kurth, W.S., Kirchner, D.L., Hospodarsky, G.B., Averkamp, T.F., Zarka, P., Lecacheux, A., Manning, R., Roux, A., Canu, P., Cornilleau-Wehrlin, N., Galopeau, P., Meyer, A., Boström, R., Gustafsson, G., Wahlund, J.-E., Åhlen, L., Rucker, H.O., Ladreiter, H.P., Macher, W., Woolliscroft, L.J.C., Alleyne, H., Kaiser, M.L., Desch, M.D., Farrell, W.M., Harvey, C.C., Louarn, P., Kellogg, P.J., Goetz, K., Pedersen, A., 2004. The radio and plasma wave science investigation. Space Sci. Rev. 114, 395.
Horányi, M., 1996. Charged dust dynamics in the Solar System. Annu. Rev. Astrophys. 34, 383–418.
Horányi, M., Juhaśz, A., Morfill, G.E., 2008. Large-scale structure of Saturn's E-ring. Geophys. Res. Lett. 35, L04203.
Jacobsen, K.S., Wahlund, J.-E., Pedersen, A., 2009. Cassini Langmuir probe measurements in the inner magnetosphere of Saturn. Planet. Space Sci. 57, 48–52.
Juhász, A., Horányi, M., Morfill, G.E., 2007. Signatures of the Enceladus plumes in Saturn's E-ring. Geophys. Res. Lett. 34, L09104.
Nicholson, P.D., Showalter, M.R., Dones, L., 1996. Observations of Saturn's ring-plane crossing in August and November. Science 272, 509–516.
Kempf, S., Beckmann, U., Moragas-Klostermeyer, G., Postberg, F., Srama, R., Economou, T., Schmidt, J., Spahn, F., Grün, E., 2008. The E ring in the vicinity of Enceladus. Spatial distribution and properties of the ring particles. Icarus 193, 420–437.
Kempf, S., Beckmann, U., Srama, R., Horányi, M., Auerd, S., Grün, E., 2006. The electrostatic potential of E ring particles. Planet. Space Sci. 54, 999–1006.
Kurth, W.S., Averkamp, T.F., Gurnett, D.A., Wang, Z., 2006. Cassini RPWS observations of dust in Saturn's E ring. Planet. Space Sci. 54, 988–998.
de Pater, I., Martin, S.C., Showalter, M.R., 2004. Keck near-infrared observations of Saturn's E and G rings during Earth's ring plane crossing in August 1995. Icarus 172, 446–454.
Richardson, J., 1995. An extended plasma model for Saturn. Geophys. Res. Lett. 22, 1177–1180.

Schmidt, J., Brilliantov, N., Spahn, F., Kempf, S., 2008. Slow dust in Enceladus' plume from condensation and wall collisions in tiger stripe fractures. Nature 451, 685–688.

Sittler Jr., E.C., Thomsen, M., Chornay, D., Shappirio, M.D., Simpson, D., Johnson, R.E., Smith, H.T., Coates, A.J., Rymer, A.M., Crary, F., McComas, D.J., Young, D.T., Reisenfeld, D., Dougherty, M., Andre, N., 2005. Preliminary results on Saturn's inner plasmasphere as observed by Cassini: comparison with voyager. Geophys. Res. Lett. 32, 14.

Spahn, F., Albers, N., Hörning, M., Kempf, S., Krivov, A.V., Makuch, M., Schmidt, J., Seiß, M., Sremčević, M., 2006a. E ring dust sources: implications from Cassini's dust measurements. Planet. Space Sci. 54, 1024–1032.

Spahn, F., Schmidt, J., Albers, N., Hörning, M., Makuch, M., Seiß, M., Kempf, S., Srama, R., Dikarev, V., Helfert, S., Moragas-Klostermeyer, G., Krivov, A.V., Sremčević, M., Tuzzolino, A.J., Economou, T., Grün, E., 2006b. Cassini dust measurements at Enceladus and implications for the origin of the E ring. Science 311, 1416–1418.

Srama, R., Ahrens, T.J., Altobelli, N., Auer, S., Bradley, J.G., Burton, M., Dikarev, V.V., Economou, T., Fechtig, H., Görlich, M., Grande, M., Graps, A., Grün, E., Havnes, O., Helfert, S., Horanyi, M., Igenbergs, E., Jessberger, E.K., Johnson, T.V., Kempf, S., 2004. The Cassini cosmic dust analyser. Space Sci. Rev. 114, 465–518.

Wahlund, J.-E, Andre, M., Eriksson, A.I.E., Lundgren, M., Morooka, M.W., Shafiq, M., Averkamp, T.F., Gurnett, D.A., Hospodarsky, G.B., Kurth, W.S., Jacobsen, K.S., Pedersen, A., Farrell, W., Ratynskaia, S., Piskunov, N., 2009. Detection of dusty plasma near the E-ring of Saturn. Planet. Space Sci., this issue, doi:10.1016/j.pss.2009.03.011.

Wahlund, J.-E., Bostrom, R., Gustafsson, G., Gurnett, D.A., Kurth, W.S., Averkamp, T., Hospodarsky, G.B., Persoon, A.M., Canu, P., Pedersen, A., Desch, M.D., Eriksson, A.I., Gill, R., Morooka, M.W., Andre, M., 2005. The inner magnetosphere of Saturn: Cassini RPWS cold plasma results from the first encounter. Geophys. Res. Lett. 32, L20S09.